Molecular-dynamics simulations of void collapse in shocked model-molecular solids

J. W. Mintmire, D. H. Robertson,* and C. T. White
Code 6179, U.S. Naval Research Laboratory, Washington, D.C. 20375-5342
(Received 4 November 1993; revised manuscript received 15 February 1994)

We have carried out a series of molecular-dynamics simulations on a model three-dimensional molecular solid to study the dynamics of shock-induced collapse of void defects. Molecular-dynamics methods were used for a model system of identical particles arranged as diatomic molecules aligned with the center of mass of each molecule at fcc lattice sites, using a {111} layering for the two-dimensional boundary conditions. The diatoms were internally coupled via a harmonic potential; all other interactions were modeled with Morse potentials between all particles other than the immediate diatomic partner. Using this model, we have investigated the effect of a cylindrical void at right angles to the direction of layering (and impact). Depending on the strength of the incident shock wave, the void is found to collapse either smoothly and symmetrically (like a balloon gradually losing air), or asymmetrically and turbulently. In the latter case, we note the transient formation (for periods of several hundreds of femtoseconds) of *"hot spots"* at the void location both in terms of the local effective temperature and the vibrational energies of the diatoms.

INTRODUCTION

The transition from shock to detonation of condensed-phase energetic materials is believed to involve local *hot spots,*[1-5] regions in the heterogeneous material which under shock have a higher local temperature than the surrounding regions. A range of defect types have been studied[6-12] as candidates for these initiation sites, including structural defects such as voids and shear bands. How energy is transferred from the shock front into the internal vibrational modes, ultimately leading to chemical reactions, is one of the critical unanswered questions in studies of the predetonation process. Both molecular dynamics[6-8] and model quantum approaches[9] have been used to study this problem.

In this paper we present results from a series of molecular-dynamics simulations of the interaction of a nanometer-scale diameter cylindrical void with a shock wave propagating in a model three-dimensional molecular solid. The void is positioned transverse to the direction of shock wave propagation. The calculations reported herein included 15 056 identical particles arranged in diatomic molecules, the center of mass of each diatom roughly located at fcc lattice sites using a {111} layering in the direction of wave propagation, and periodic boundary conditions imposed in two dimensions. The system was shocked using the impact of a four-layer flyer plate. We followed the resulting effects of this impact on a range of local properties, and find the formation of local *"hot spots"* when the impact energy is sufficient to result in a turbulent collapse of the void. This paper is an extension of earlier preliminary results reported for smaller systems.[13]

APPROACH

The molecular-dynamics simulations were carried out on a model condensed-phase system constructed from an fcc lattice of 60 close-packed layers of atomic dimers stacked in a {111} direction; this direction was assigned the z axis. Periodic boundary conditions were imposed in the x and y directions (i.e., a finite number of layers having infinite extent) with the periodic unit cell containing 16 rows of 8 diatoms in each row, with the row direction aligned in the x direction.

Two types of interatomic interactions were assumed. Within each diatom the particles interacted via a harmonic potential in the diatomic bond distance r, $V_{\text{diatom}}(r) \equiv \frac{1}{2}K(r-r_0)^2$, with a spring constant $K=500$ J/m^2 and equilibrium bond distance $r_0=0.16$ nm. Each atom was assumed to have a mass of 14 amu ($\sim 2.3\times10^{-26}$ kg). These harmonic parameters and the atomic masses were chosen to approximate the behavior of bonds in organic molecules in a molecular crystal, with the spring constant roughly that of the force constant of a typical carbon-carbon single bond.[14] The harmonic potential prevents dissociation of the diatom over the course of the simulation allowing easy analysis of the vibrational energy distribution. The mass density of 0.4 g/cm^3 is less than typical molecular solids of greater than 1 g/cm^3; this low density is a consequence of the low molecular weight of this simplest molecule—a diatomic. Increasing the mass density and using diatomics would have required either an unphysically large particle mass or physically unrealistic intermolecular potentials.

Interactions between atoms in different dimers were modeled using a Morse potential with a well depth of 3.2×10^{-21} J and an equilibrium separation of 0.5 nm. These values are of the order of those typically found for van der Waals interactions in molecular crystals. A crystal with three-dimensional periodic boundary conditions corresponding to a block of $8\times12\times6$ dimers was initially constructed with the centers of mass of each diatom arranged in an fcc lattice with stacking in a {111} direction and a nearest-neighbor distance (between centers of mass) of the Morse potential separation of 0.5 nm. The diatom-

ic axes of symmetry were oriented randomly. The lattice was then brought to equilibrium using standard molecular-dynamics techniques to a zero pressure configuration at 100 K. The bulk sound velocity was estimated to be 3 km/sec using a numerical evaluation of the bulk modulus of the crystal. The relaxed nearest-neighbor equilibrium distance between centers of mass of the dimer pairs is about 0.55 nm. The shock was simulated by a finite thickness slab constructed from the {111} layers of the crystal. Two-dimensional periodicity was imposed over a region 4.2×7.5 nm, corresponding to an 8×16 pattern of dimers in a layer. The slab was about 25 nm thick (60 layers).

We chose a Cartesian coordinate system with the x and y directions along the periodic boundary repeat vectors, and the z direction normal to the {111} layering. A cylindrical void with a diameter of about 2.0 nm of of 152 pairs per periodic cell (with the central axis of the cylinder lying parallel to the x axis) was removed from the system. The atomic trajectories were calculated using a standard leap-frog algorithm with a 0.5-fs time step. All atoms started with an initial distribution of velocities with an average kinetic temperature of 100 K. Shock waves have been simulated by using layers 1–4 as a flyer plate, moving the plate back by 0.2 nm and adding impact velocities of varying magnitudes to the initial velocities of the atoms in the plate. The representative examples that we discuss herein used impact velocities of 3, 5, and 7 km/sec.

We have calculated several local properties using the approach of Hardy,[15] assuming a Gaussian broadening function with a full width at half maximum (FWHM) of 0.2 nm. This length scale was chosen because it is roughly half the diatomic center-of-mass spacing of about 0.5 nm. This choice leads to a reasonably smooth depiction of data without completely blurring out the effect of individual diatomic molecules. The local particle density is then given by a sum of Gaussian distribution functions $f(r)$ centered about the nuclear positions $\mathbf{r}_i$

$$\rho(\mathbf{r})=\sum_i f(|\mathbf{r}-\mathbf{r}_i|)\ . \tag{1}$$

For properties dependent directly on atomic positions, such as the local particle velocity, the local property is then calculated

$$\mathbf{v}(\mathbf{r})=\frac{\sum_i f(\mathbf{r}-\mathbf{r}_i)\mathbf{v}_i}{\sum_i f(\mathbf{r}-\mathbf{r}_i)}\ . \tag{2}$$

For a local property X dependent on bonds (i.e., on interatomic separation), we estimate the local properties by defining a local bond contribution X_{ij} for the bond between atomic sites i and j. We then split this bond contribution between the two end points equally and Gaussian broaden as before. Thus for a generic property $X(\mathbf{r})$ with bond contributions X_{ij}

$$X(\mathbf{r})=\frac{\sum_{i<j}\frac{1}{2}[f(\mathbf{r}-\mathbf{r}_i)+f(\mathbf{r}-\mathbf{r}_j)]X_{ij}}{\sum_i f(\mathbf{r}-\mathbf{r}_i)}\ . \tag{3}$$

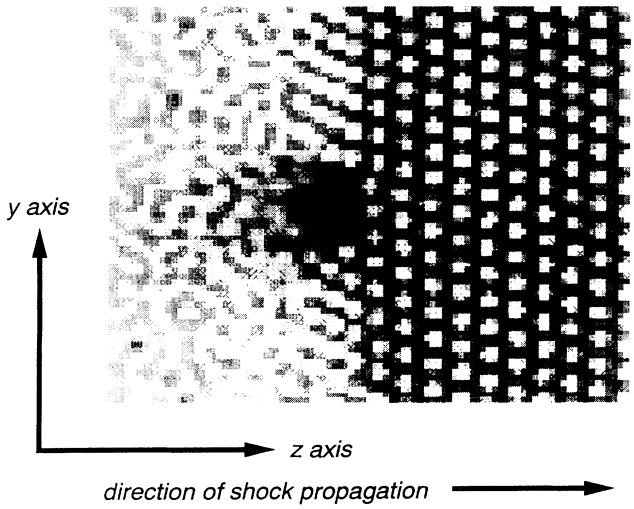

FIG. 1. Shapshot of two-dimensional average of the local particle density over 91×71 grid (8 nm $\times$7nm) for 7-km/sec impact velocity simulation at 1.1 ps. Dark areas denoted low density and light areas denote high density. Note ordered regions to right of figure where shock front has not yet reached.

As an estimate of the local vibrational energy, we therefore define X_{ij} using the sum of the diatomic bond-stretch contribution to the kinetic energy and the potential energy of the diatomic bond,

$$X_{ij}=\frac{M}{4}\frac{[(\mathbf{v}_i-\mathbf{v}_j)\cdot(\mathbf{r}_i-\mathbf{r}_j)]^2}{|\mathbf{r}_i-\mathbf{r}_j|^2}+\frac{1}{2}K|\mathbf{r}_i-\mathbf{r}_j|^2\ . \tag{4}$$

The local hydrostatic pressure is likewise estimated using the defining relationship

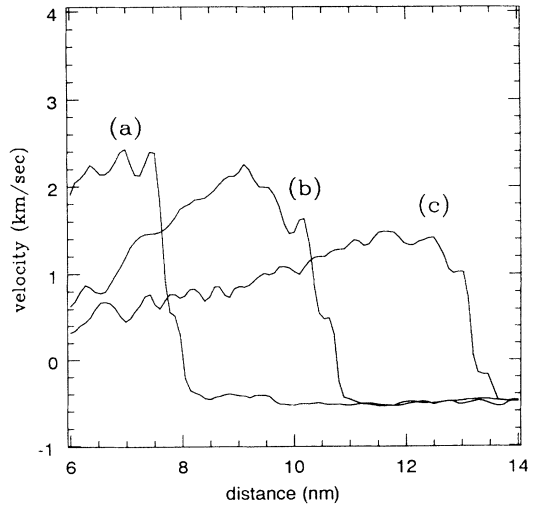

FIG. 2. Snapshots of z component (direction of shock front propagation) of local particle velocities along line bisecting void defect for 7-km/sec impact velocity simulation at times of (a) 0.8 ps, (b) 1.2 ps, and (c) 1.6 ps.

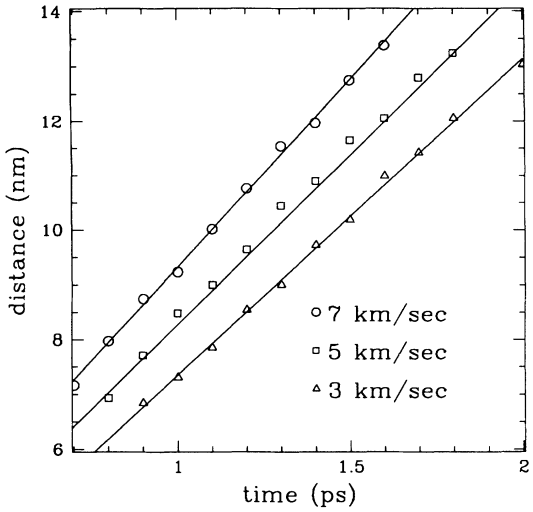

FIG. 3. Location of shock front as a function of time for the (circles) 7-km/sec impact velocity simulations, (squares) 5-km/sec impact velocity simulations, and (triangles) 3-km/sec impact velocity simulations.

$$P=-\frac{\partial E}{\partial V}=-\frac{1}{3V}\sum_{i<j} r_{ij}\phi'_{ij}(r_{ij})\ , \tag{5}$$

where $\phi_{ij}(r_{ij})$ is the interatomic potential between atoms i and j as a function of bond distance r_{ij}, and ϕ' is the derivative with respect to the bond distance.

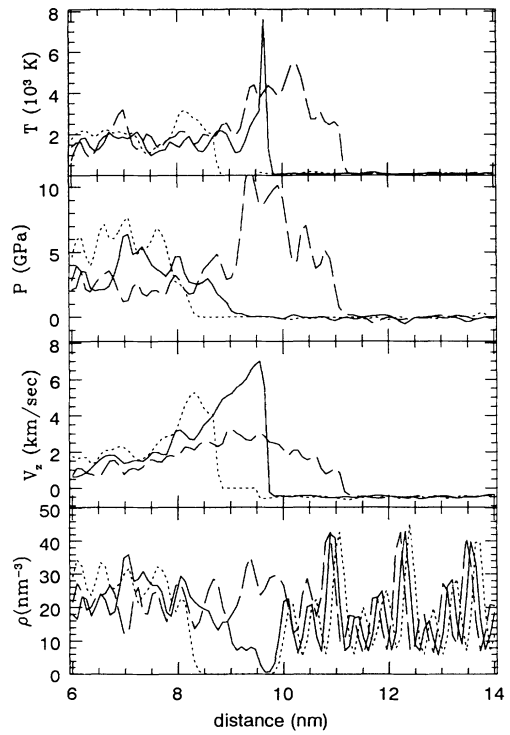

FIG. 4. Local particle density (ρ), z component of local particle velocity (V_z), local hydrostatic pressure (P), and effective kinetic temperature (T) for 7-km/sec impact velocity simulation along central line bisecting void defect at simulation times 0.9 ps (dotted lines), 1.1 ps (solid lines), and 1.3 ps (dashed lines).

RESULTS

Because of the relative homogeneity of the system along the x axis (parallel to the cylinder axis), we have averaged over this direction to reduce all local properties to two-dimensional fields. In particular, we have calculated the local density, kinetic energy, z component of the particle velocity, vibrational energy, and hydrostatic pressure on a 91×71 grid spanning an 8 nm $\times$7 nm rectangular section of the y-z plane. In Fig. 1 we depict a gray-scale representation of the local density calculated using the above-described algorithm for an flyer-plate impact velocity of 7 km/sec at 1.1 ps into the simulation, immediately before the void collapses. Because the x direction lies along the close-packed rows of the fcc lattice, we can still see the location of these rows on the right-hand side of Fig. 1 (as the lighter shaded regions) even after the averaging in the x dimension. The shock front is sharp on an atomic scale as anticipated by continuum theory[16] and verified by earlier molecular-dynamics simulations,[17–22] and the disorder induced by the front is evident in the left-hand side of the figure.

In Fig. 2 we depict averages over the x-y plane (obtained by averaging over the 71 values calculated for the two-dimensional grid at a given value of z) of the z component of the atomic velocities as a function of the z

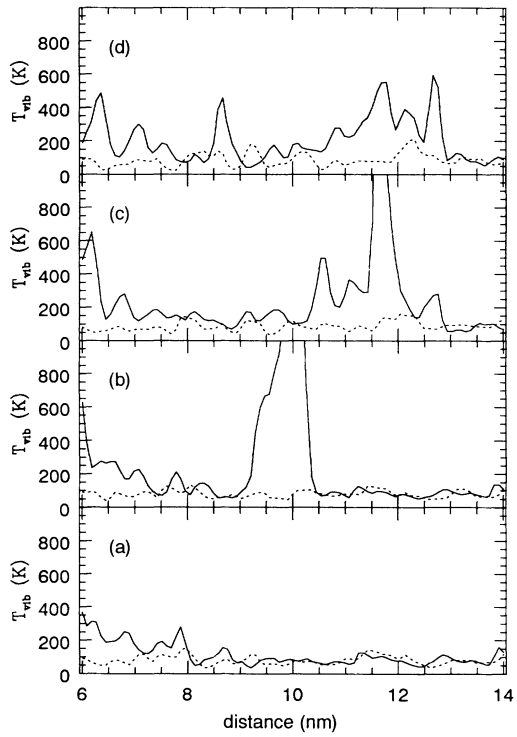

FIG. 5. Snapshots of effective vibrational temperature, $T_{\rm vib}$, along central line bisecting void defect. Solid lines depict results for 7-km/sec impact velocity simulation at times (a) 1.1 ps, (b) 1.2 ps, (c) 2.4 ps, and (d) 3.6 ps. Dashed lines depict results for 3-km/sec impact velocity simulation at times (a) 1.8 ps, (b) 1.9 ps, (c) 2.4 ps, and (d) 3.6 ps. Note that (a) and (b) represent times immediately before and immediately after void closure in both simulations.

coordinate for an impact velocity of 7 km/sec at three times. We note that the void is initially centered at a z coordinate of roughly 10 nm. We see from inspection of Fig. 2 that the wave front velocity is approximately 6–7 km/sec, substantially faster than the sound velocity of 3 km/sec. This velocity will decrease as energy is dissipated by the shock front in the unreactive model-molecular solid, but over the time and distance scales in our simulation this effect is minor. As expected, the average particle velocities are slower than the shock velocity. The 5- and 3-km/sec impact simulations also have shock front velocities of near 6 km/sec, and only slightly slower than that of the 7-km/sec impact simulation. Figure 3 depicts the estimated location of the wave front for all three simulations as a function of time, obtained by visual inspection of particle velocity curves such as those in Fig. 2. These results imply wave front velocities of 5.8, 6.2, and 6.9 km/sec for impact velocities of 3, 5, and 7 km/sec, respectively. In other simulations with slower impact velocities, we find that the wave front velocity continues to decrease. These results are similar to those we have obtained using more sophisticated bond-order potentials in two-dimensional simulations.[19–22]

Figure 4 depicts the local density, z component of the particle velocity, pressure, and effective kinetic temperature, T_K (defining T_K so that $3k_B T_K/2$ equals the local

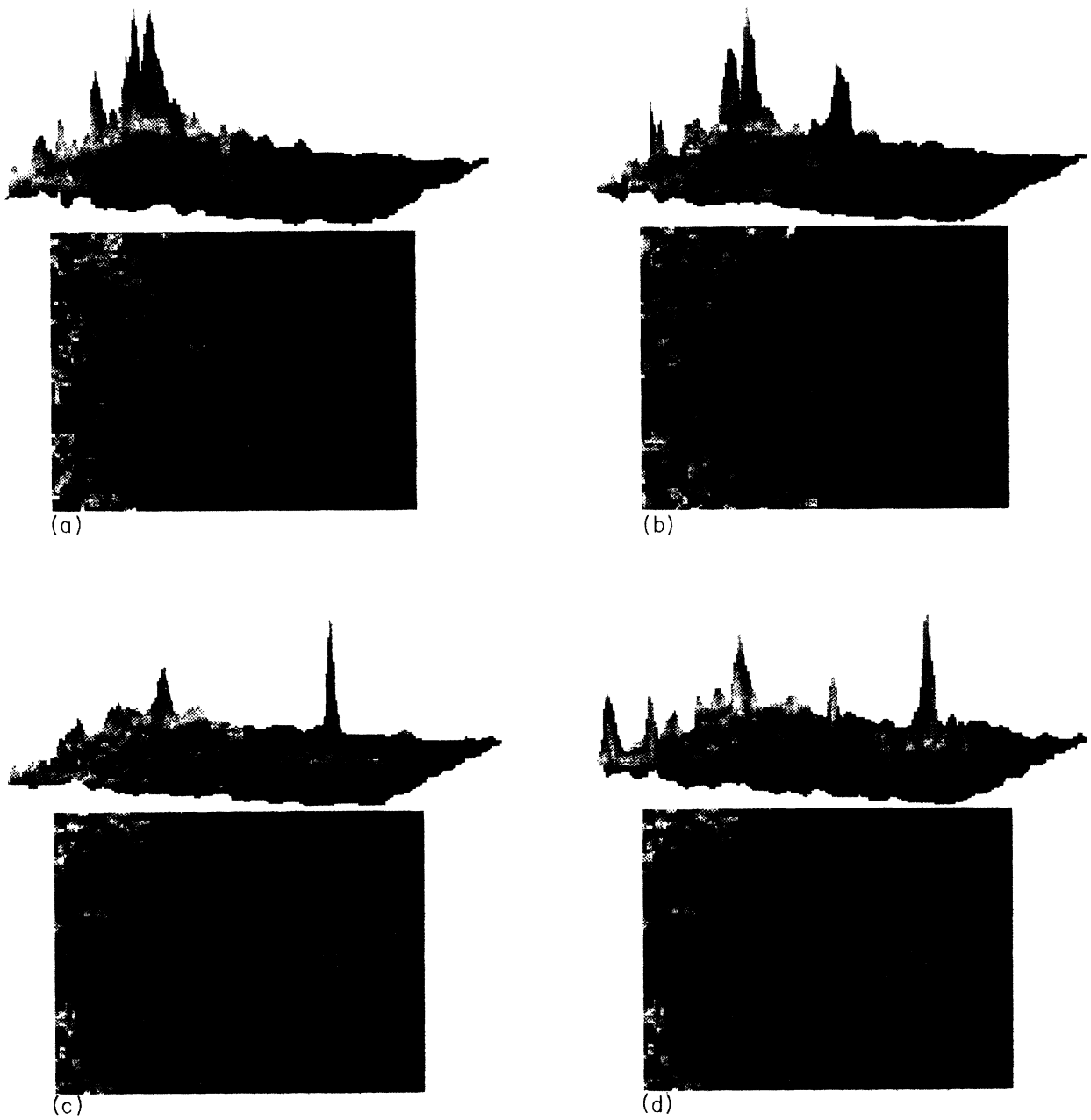

FIG. 6. Color depiction of two-dimensional representation of local effective vibrational effective temperature in the vicinity of void defect for 7-km/sec impact velocity simulation at times (a) 1.1 ps, (b) 1.2 ps, (c) 2.4 ps, and (d) 3.6 ps. The color scale corresponds to blue for low temperature and red for $T_{\text{vib}} > 500$ K.

kinetic energy per particle) for the 7-km/sec impact velocity simulation at simulation times of 0.9, 1.1, and 1.3 ps. These simulation times correspond to times before the wave front reaches the void, immediately before the void collapses, and immediately after the wave front collapses, respectively. These data represent an average along a narrow line extending parallel to the z coordinate axis and intersecting the central axis of the void. That is, rather than reduce the two-dimensional data to a one-dimensional curve by averaging over all the calculated data points at a given z coordinate, we have averaged over a 0.2-nm-wide strip that bisects the cylindrical void.

The pressure and particle velocity profiles for the 1.1-ps snapshot, just as the void is collapsing, are similar to those found for the collapse of a bubble.[23] In particular we note that the sharp front and rapidly decreasing tail of the particle velocity as we look further back in the wave front, while the pressure rises gradually from zero. These particles in the void have been accelerated by the wave front to velocities comparable to the wave front velocity, essentially ejected into the void.

The data for the 1.3-ps snapshot show the aftermath of the collapse of the void: the ejected material strikes the rear wall of the void at high velocities. As can be seen in Fig. 4, this leads to a region at the rear wall of the void with relatively high pressures and kinetic temperatures, similar to results in continuum mechanics simulations of finite-length cylindrical and spherical voids in a shocked solid by Mader.[24] Figures 5 and 6 depict the local effective vibrational temperature $T_{\rm vib}$ [defined by setting $k_B T_{\rm vib}$ equal to the local vibrational energy calculated using Eq. (4)] for the 7-km/sec impact velocity simulation at simulation times of 1.1, 1.2, 2.4, and 3.6 ps, respectively. Figure 5 shows the local vibrational temperature, a measure of the excitation of the "internal" bond vibrational mode of the dimers, along a line bisecting the void; results for the 3-km/sec impact are also shown for comparison in dotted lines. In the 7-km/sec impact velocity simulation we see little excitation of the vibrational modes until the void collapses. Figure 6 shows a full two-dimensional representation of the vibrational temperature; the excitation of the vibrational mode is seen to be localized at the rear wall of the void. The disintegration of the front wall of the void leads to lattice disruption, and the resulting collision on the rear wall leads to a strong coupling of the internal vibrational modes of the material to the wave front.[7] Because of the weak coupling of the internal vibrational modes with the lattice and the shock front, this *hot spot* remains present for extended times and only slowly cools compared to the time required for the shock wave front to pass by the void. Even at 3.6 ps we can see the remnants of the original vibrational hot spot.

For the weaker impact simulations we find little vibrational excitation. We observe a transient increase in the local kinetic energy in the vicinity of the void as it collapses in the weaker impact simulations, but this increase dissipates over a period of roughly 1 ps to that expected if no void were present and leads to no enhanced excitation of the vibrational modes. Furthermore, while the local kinetic temperature increases to several thousand degrees K in our simulation, the local vibrational temperature remains an order of magnitude less than the kinetic temperatures, except in the vicinity of the collapsed void in the 7-km/sec impact simulation. The appropriate relaxation time (or up-pumping time) for excitation of the stiff intramolecular vibrational modes, with their weak coupling to the intermolecular lattice vibrational modes, is expected to require times on the order of 10–50 ps (Ref. 9)—substantially longer than the simulation times presented herein. In a longer time scale, we would expect these temperatures to equilibrate. In the weaker impact simulations where we see little vibrational excitation, the particle velocities of the wave front that collapses the void are found to be of the same magnitude as the average particle velocities in the shock front—the void wall maintains sufficient cohesion to collapse smoothly rather than the turbulent collapse found in the stronger impact simulations. We thus note in our simulations that excitation of vibrational modes coincides with the breakdown of the lattice, i.e., ejection of material into the void, and we speculate that this turbulent disintegration of the void wall and ejection of material into the void are a necessary antecedent to excitation of the internal vibrational modes.

SUMMARY

We have carried out a series of molecular-dynamics simulations on a model system to study the effects of atomic-scale voids on hot-spot formation during pressure-wave propagation in condensed-phase systems. Three-dimensional molecular-dynamics methods were used for a model system of diatomic molecules arranged in a $\{111\}$ layering of an fcc lattice. Using this model, we have investigated the effects of impact strength on the resulting excitation of the vibrational modes of the model dimer. We find that substantial excitation of the vibrational modes is obtained if the shock strength is sufficient to accelerate particles on the leading edge of the void defect to velocities comparable to the shock front velocity. In our simulations this condition leads to a turbulent collapse of the void rather than a relatively smooth and symmetric collapse of the void. These results suggest that such a turbulent collapse is instrumental in the vibrational excitation. For a nanoscale void, we find that sufficiently strong shocks can lead to direct excitation of the intramolecular vibrational modes, i.e., up-pumping these modes, on time scales much shorter than expected for these weakly coupled modes.

ACKNOWLEDGMENTS

This work was supported by the Office of Naval Research through NRL and the ONR Physics Division. Computational support for this project was supported in part by a grant of computer resources from the Naval Research Laboratory.

*Present address: Department of Chemistry, Indiana University–Purdue University at Indianapolis, Indianapolis, IN 46202-3274.

[1]J. N. Johnson, P. K. Tang, and C. A. Forest, J. Appl. Phys. **57**, 4323 (1985).

[2]J. N. Johnson, Proc. R. Soc. London, Ser. A **413**, 329 (1987).

[3]S. A. Bordzilovskii, S. M. Karakhanov, and V. F. Lobanov, Fiz. Goreniya Vzryva **23**, 132 (1987) [Combust. Explos. Shock Waves (USSR) **23**, 624 (1987)].

[4]P. K. Tang, J. Appl. Phys. **63**, 1041 (1988).

[5]F. E. Walker and A. M. Karo, in *Shock Waves in Condensed Matter,* edited by S. C. Schmidt and N. C. Holmes (Elsevier, Amsterdam, 1988), pp. 543–546.

[6]A. M. Karo and J. R. Hardy, Int. J. Quantum Chem. Symp. **20**, 763 (1986).

[7]A. M. Karo, T. M. Deboni, J. R. Hardy, and G. A. Weiss, Int. J. Quantum Chem. Symp. **24**, 277 (1990).

[8]D. H. Tsai, in *Chemistry and Physics of Energetic Materials,* Vol. 309 of *NATO Advanced Study Institute, Series C,* edited by S. N. Bulusu (Kluwer, Dordrecht, 1990), pp. 195–227; D. H. Tsai, J. Chem. Phys. **95**, 7497 (1991).

[9]D. D. Dlott and M. D. Fayer, J. Chem. Phys. **92**, 2798 (1990); A. Tokmakoff, M. D. Fayer, and D. D. Dlott, *ibid.* **97**, 1901 (1993).

[10]C. S. Coffey, J. Phys. (Paris) Colloq. **48**, C4-253 (1987).

[11]F. A. Bandak, D. H. Tsai, R. W. Armstrong, and A. S. Douglas, Phys. Rev. B **47**, 11 681 (1993).

[12]F. A. Bandak, R. W. Armstrong, and A. S. Douglas, Phys. Rev. B **46**, 3228 (1992).

[13]J. W. Mintmire, D. H. Robertson, D. W. Brenner, and C. T. White, in *Shock Compression of Condensed Matter 1991,* edited by S. C. Schmidt, R. D. Dick, J. W. Forbes, and D. G. Tasker (Elsevier, Amsterdam, 1992), pp. 147–150.

[14]D. W. Brenner, Phys. Rev. B **42**, 9458 (1990).

[15]R. J. Hardy, J. Chem. Phys. **76**, 622 (1982).

[16]Ya. B. Zel'dovich and Yu. R. Raizer, *Physics of Shock Waves and High-Temperature Hydrodynamic Phenomena* (Academic, New York, 1967), Vol. 1, pp. 45–49.

[17]B. L. Holian, W. G. Hoover, W. Moran, and G. K. Staub, Phys. Rev. A **22**, 2798 (1980).

[18]A. N. Dremin and V. Yu. Klimenko, Prog. Astronaut. Aeronaut. **75**, 253 (1981).

[19]D. H. Robertson, D. W. Brenner, and C. T. White, Phys. Rev. Lett. **67**, 3132 (1991).

[20]C. T. White, D. H. Robertson, M. L. Elert, and D. W. Brenner, in *Microscopic Simulations of Complex Hydrodynamic Phenomena,* edited by M. Mareschal and B. L. Holian (Plenum, New York, 1992), pp. 111–123.

[21]D. W. Brenner, D. H. Robertson, M. L. Elert, and C. T. White, Phys. Rev. Lett. **70**, 2174 (1993).

[22]C. T. White, D. H. Robertson, and D. W. Brenner, Physica A **188**, 357 (1992).

[23]Ya. B. Zel'dovich and Yu. R. Raizer, *Physics of Shock Waves and High-Temperature Hydrodynamic Phenomena* (Academic, New York, 1967), Vol. 2, pp. 807–812.

[24]C. L. Mader, *Numerical Modeling of Detonations* (University of California Press, Berkeley, 1979), Chap. 3.

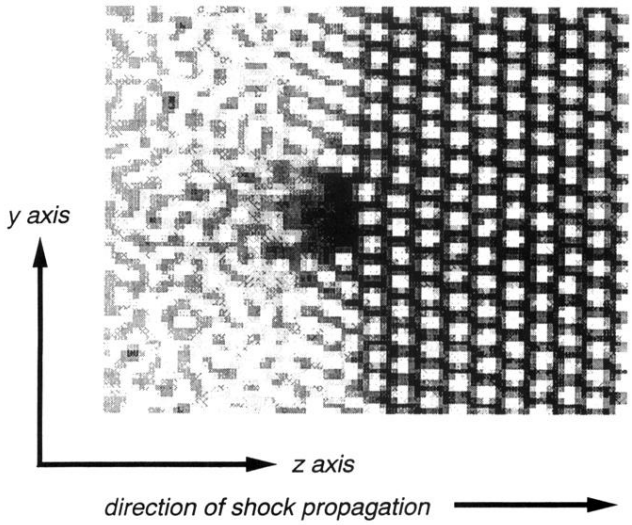

FIG. 1. Shapshot of two-dimensional average of the local particle density over 91×71 grid (8 nm ×7nm) for 7-km/sec impact velocity simulation at 1.1 ps. Dark areas denoted low density and light areas denote high density. Note ordered regions to right of figure where shock front has not yet reached.

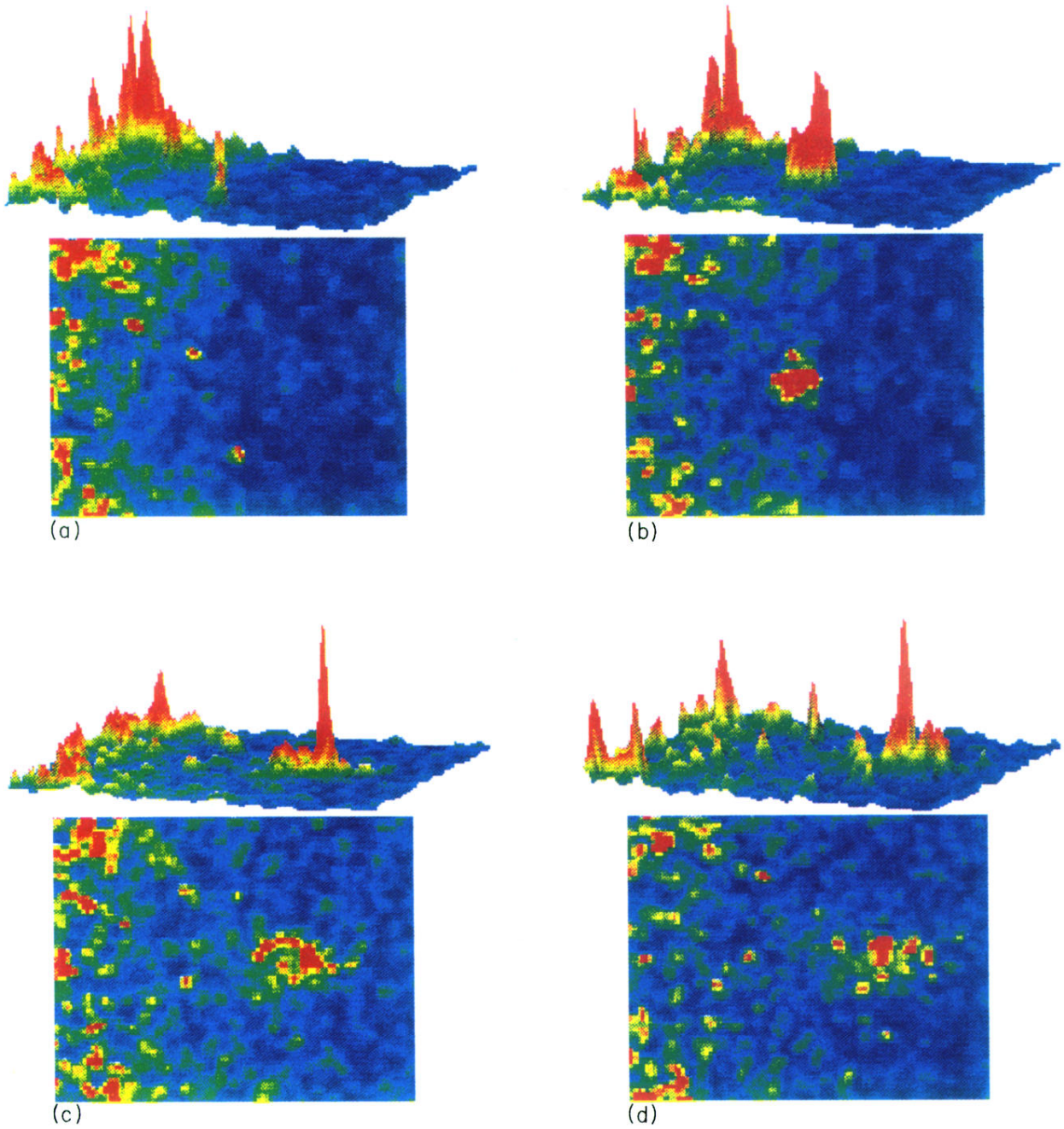

FIG. 6. Color depiction of two-dimensional representation of local effective vibrational effective temperature in the vicinity of void defect for 7-km/sec impact velocity simulation at times (a) 1.1 ps, (b) 1.2 ps, (c) 2.4 ps, and (d) 3.6 ps. The color scale corresponds to blue for low temperature and red for $T_{\text{vib}} > 500$ K.